Heavy residues following 5—10 MeV/nucleon ^{12}C- and ^{14}N-induced reactions on Sm and Pr targets

R. Kossakowski
Institute for Nuclear Research, Swierk near Warsaw, Poland
and Institut des Sciences Nucléaires, F-38026 Grenoble-Cedex, France

J. Jastrzębski,* P. Rymuza,† and W. Skulski*
Institute for Nuclear Research, Swierk near Warsaw, Poland

A. Gizon, S. André, J. Genevey, J. Gizon, and V. Barci
Institut des Sciences Nucléaires, F-38026 Grenoble-Cedex, France
(Received 30 January 1985)

The individual evaporation residue cross sections have been measured for ^{12}C- and ^{14}N-induced reactions on ^{141}Pr and $^{144,147,150,152,154}Sm$ targets at incident energies of 5 to 10 MeV/nucleon. Gamma-ray detection techniques were used. The competition between neutron, charged particle, and gamma-ray emission was studied as a function of the excitation energy, angular momentum, and the distance of the compound nucleus from the stability line. The general behavior of the mass and charge distributions of the reaction residues is in agreement with complete fusion-evaporation calculations, but some aspects of the data point to a small contribution of other reaction mechanisms.

I. INTRODUCTION

Many experimental and theoretical works have been devoted to the study of formation and decay of the highly excited systems in heavy-ion collisions at energies below 10 MeV/nucleon (see, e.g., Refs. 1 and 2 and references quoted therein). In spite of the fact that the major properties of fusion-fission or evaporation are now quite well understood, systematic studies covering a large number of compound nuclei (CN), excitation energies, or projectiles are not very abundant. In particular, only a few experimental works[3,4] were devoted to the quantitative studies of the influence of the neutron deficiency of the CN on the competition between neutron and charged particle emission. The detailed knowledge of this effect is important when attempts are made to produce isotopes far removed from the beta stability line. This influence may be best studied for target elements which possess a large number of stable isotopes, as is the case for Sm targets. The interest of performing experiments for compound nuclei in the $A \approx 160$ mass region is increased by the fact that relatively high angular momenta may contribute to the production of evaporation residues[5] before fission occurs.[6]

In this paper we present an extensive study of the competition between neutron, charged particle, and gamma ray emission from compound nuclei in a large domain of excitation energies, angular momenta, and CN neutron to proton ratios. For this purpose a number of Sm and Pr targets were bombarded with ^{12}C and ^{14}N projectiles from the variable energy cyclotron in Grenoble. The residual product cross sections were determined by on-line gamma-ray spectroscopic techniques. The gamma-ray detection for this kind of experiment was also used by others (see, e.g., Refs. 7—11).

The experimental results cover a fairly large domain of compound nuclei, from neutron-rich systems mainly deexciting by neutron and gamma-ray emission, to very neutron-deficient ones for which charged particle emission dominates. These results are presented in terms of evaporation: removed mass ΔA, charge ΔZ, and neutron number ΔN as a function of the excitation energy, entrance channel angular momentum, and distance of the compound nucleus from the beta stability line. A number of systematic trends are distinguished and compared with heavier projectiles. A simple discussion of the angular momentum effects is followed by a more detailed comparison of the experimental data with two different evaporation codes, ALICE (Refs. 12 and 13) and LANCELOT (Refs. 14—16). Some indications of the occurrence of processes other than complete fusion are obtained by comparing the results for the ^{12}C and ^{14}N projectiles.

The experimental data presented in this paper were partly gathered during the search and identification of the high-spin isomers in the investigated mass region.[17] The measurements of the intensities of gamma rays, prompt and delayed with respect to the beam pulse, as a function of the bombarding energy, cross bombardments, gamma-gamma coincidence experiments, and the determination of the prompt and delayed gamma-ray multiplicity made an unambiguous identification possible for most of the observed gamma lines. Preliminary or partial results of the present study were presented previously.[18—20]

II. EXPERIMENTAL PROCEDURE

Self-supporting, isotopically enriched targets of ^{144}Sm, ^{147}Sm, ^{150}Sm, ^{152}Sm, and ^{154}Sm and a natural target of

^{141}Pr were prepared from metallic samples rolled under argon atmosphere.[21] Their thicknesses ranged from 5 to 18 mg/cm^2. These targets were irradiated with ^{12}C and ^{14}N beams. The typical irradiation time for a beam current of 0.3 particle nA was about 2 h. The incident energy was varied from 71 to 110 MeV for ^{12}C ions and from 68 to 120 MeV for ^{14}N ions. The experimental conditions are given in Table I.

The experiment consisted of measurements of gamma rays prompt and delayed with respect to the beam. Natural beam pulsing in the nanosecond range and millisecond pulsation of the ion source were used. The gamma rays were recorded by three Ge(Li) detectors and a multiplicity setup consisting of 14 NaI(Tl) counters.

The first Ge(Li) detector of about 10% absolute efficiency and 2.2 keV energy resolution for ^{60}Co lines was placed at 125° with respect to the beam direction, at 10 cm from the target. Its efficiency was calibrated against standard sources with an accuracy higher than 5%. This detector was used for the determination of the absolute intensities of gamma rays during the beam irradiation and immediately after the beam shut-off.

At 55° a small planar detector was placed at a distance of 20 cm from the target. This detector recorded simultaneously with the first Ge(Li) counter the fluorescent K x rays of the target atoms and the low energy gamma rays. The intensity of the K x rays, corrected for absorption in the target (correction typically of the order of 5%), served for the cross-section normalization of the gamma rays recorded in both Ge(Li) detectors. The cross section

TABLE I. Experimental bombarding conditions.

Beam	Target	E_{lab} (MeV)	$\bar{E}_{lab}$[a] (MeV)	CN	$\bar{E}^{*}_{CN}$[b] (MeV)	Target thickness (mg/cm^2)
^{12}C	^{144}Sm	82	73.5	^{156}Er	49.6	18
		90	81.9		57.4	
		98	90.3		65.2	
		110	102.5		76.5	
	^{147}Sm	90	85.2	^{159}Er	63.9	10
		98	93.4		71.4	
		110	105.8		82.9	
	^{150}Sm	90	85.2	^{162}Er	68.2	11
		110	105.8		87.3	
	^{152}Sm	71	65.5	^{164}Er	51.8	12
		90	85.2		70.1	
		98	93.4		77.7	
		110	105.8		89.2	
	^{154}Sm	90	88.0	^{166}Er	74.1	5
		110	108.0		92.6	
	^{141}Pr	82	77.4	^{153}Tb	56.6	10
		90	85.5		64.1	
		98	93.8		71.7	
		110	106.1		83.1	
^{14}N	^{144}Sm	80	66.5	^{158}Tm	39.9	18
		95	83.0		54.9	
		107	96.0		66.8	
	^{147}Sm	80	73.0	^{161}Tm	51.9	10
		95	88.5		66.0	
		107	101.0		77.4	
		120	114.5		89.7	
	^{150}Sm	80	72.0	^{164}Tm	53.7	11
		95	88.0		68.3	
		107	100.5		79.7	
		120	114.0		92.1	
	^{152}Sm	80	71.0	^{166}Tm	55.0	12
		95	87.0		69.7	
		107	100.0		81.6	
		120	113.5		93.9	
	^{141}Pr	68	59.5	^{155}Dy	40.1	10
		80	72.5		52.0	
		95	88.0		66.1	
		107	101.0		77.9	
		120	114.0		89.7	

[a]Energy of the beam at half-thickness of the target.
[b]Average excitation energy of the compound nucleus.

for the K-shell ionization of target atoms was calculated using the plane-wave Born approximation (PWBA) with a number of corrections. The details of the normalization procedure are presented in the Appendix.

The third Ge(Li) detector at 90°, similar to the first one, worked in coincidence with the multiplicity setup. The relative intensities of the gamma lines from this detector, collected in a zerofold, onefold, twofold, and greater-than-or-equal-to-threefold coincidence with the 14 NaI(Tl) counters were transformed into the multiplicity of the corresponding gamma cascades. The details of data acquisition and evaluation were reported in Ref. 22.

The pulses from the Ge(Li) counters were sent, through the 200 MHz analog-to-digital converters (ADC's), to three independent multichannel analyzers and were routed to different parts of their memory according to the timing conditions with respect to the beam pulse and, for the third Ge(Li), also fold conditions. About 400 spectra ($2K$ and $4K$ each) were recorded and analyzed[23] in this work.

III. ANALYSIS OF THE DATA

A. Evaluation of the cross sections from the in-beam gamma ray spectra

An example of gamma-ray spectra collected during the beam bursts is presented in Fig. 1 for the $^{14}N+^{141}Pr$ reaction at five different bombarding energies. The ^{152}Dy, ^{151}Dy, ^{150}Dy, and ^{149}Dy lines, dominating the 68, 80, 95, and 107 MeV spectra, respectively, are clearly seen. The lines of ^{150}Tb, ^{149}Tb and ^{147}Gd, ^{146}Gd, and ^{145}Gd appear at higher energies.

The peak to background ratio deteriorates with increasing incident beam energy. This effect, due to the increasing gamma-ray multiplicity and broader distribution of the residual nuclei, makes the identification more difficult and increases the errors of the calculated peak areas. For example, the production cross sections of the ^{152}Dy nucleus at 68 MeV and of the ^{149}Tb nucleus at 120 MeV are similar (100±20 mb and 110±50 mb, respectively), and

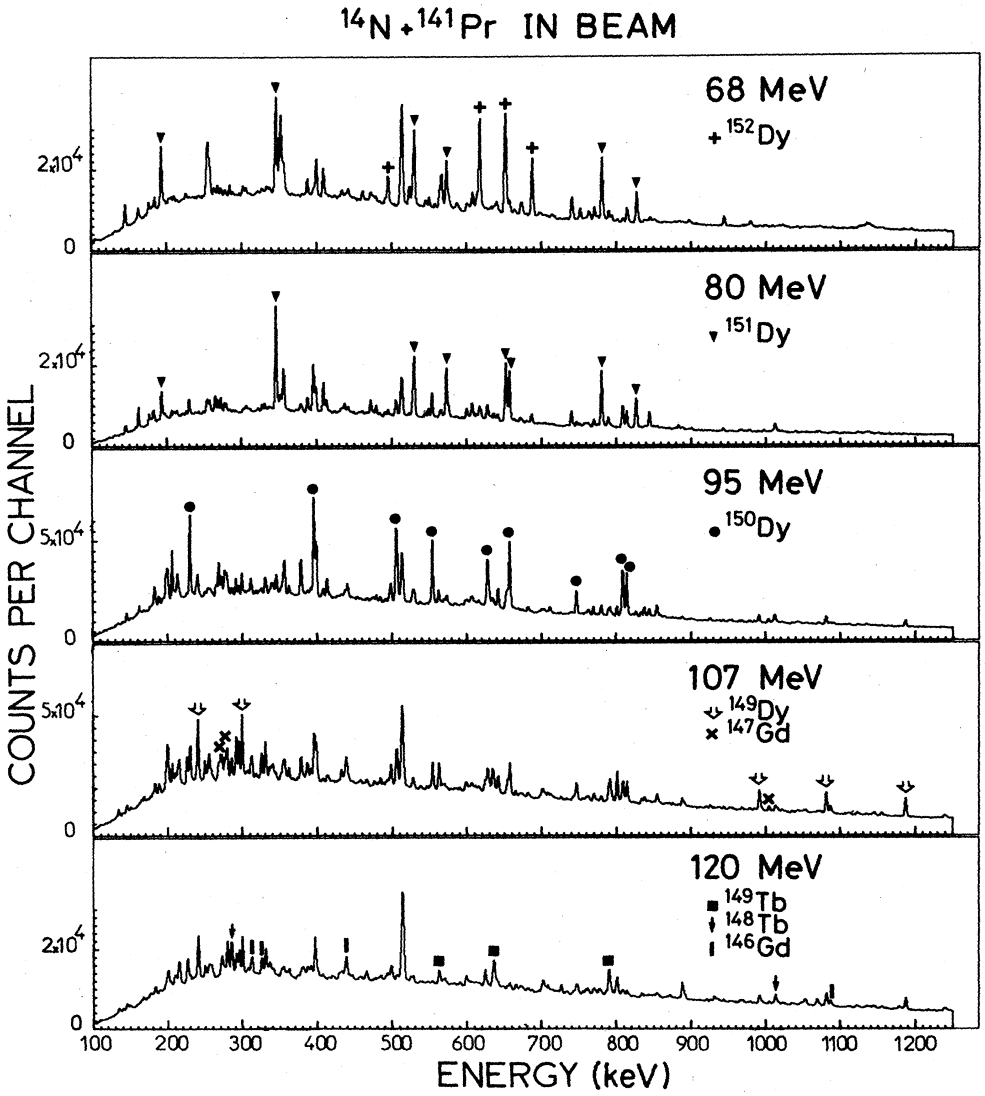

FIG. 1. Gamma-ray spectra following the $^{14}N+^{141}Pr$ reaction collected during the beam bursts at 68, 80, 95, 107, and 120 MeV bombarding energies. Only the strongest lines are explicitly indicated in the figure.

the main part of the gamma flow goes through a single yrast cascade for both nuclei. One observes (Fig. 1) very well-pronounced peaks in the case of ^{152}Dy, whereas the ^{149}Tb lines are much weaker with respect to the background in the 120 MeV spectrum.

The ground-state production cross sections were determined from the in-beam gamma-transition intensities corrected for the side-feeding and summing effect. In heavy-ion fusion reactions the residual nuclei are usually produced with high angular momenta and the main gamma flow passes along the yrast cascade (with possible exceptions for some odd-odd nuclei). The weak side-feeding in the low spin region can then be easily estimated and reliable corrections made. The correction for summing in the Ge(Li) detector depending on the gamma-ray multiplicity and total efficiency of the detector was made according to Ref. 24. This correction was usually of the order of 20%.

The identification of the in-beam gamma lines was based on the existing literature data, completed by the results obtained during a search for high spin isomers in this region.[17] The levels of light Tm isotopes ($A \leq 157$) were identified in a separate experiment, and their preliminary level schemes are presented in Fig. 3. Level schemes of heavier Tm isotopes ($A \geq 158$) were recently reported.[25–28]

B. Evaluation of the cross sections from the radioactive decays

The in-beam gamma-ray measurements were supplemented by radioactivity measurements of short-lived isotopes abundantly formed in the investigated mass region. Delayed spectra were collected under the same conditions as the in-beam data but during the off-beam time in nanosecond and millisecond beam pulsing. Figure 2 presents an example of such spectra collected between the nanosecond beam bursts for the reaction $^{14}N+^{141}Pr$. The observed transitions originate from various isomers excited in this reaction and from the radioactive decay of the

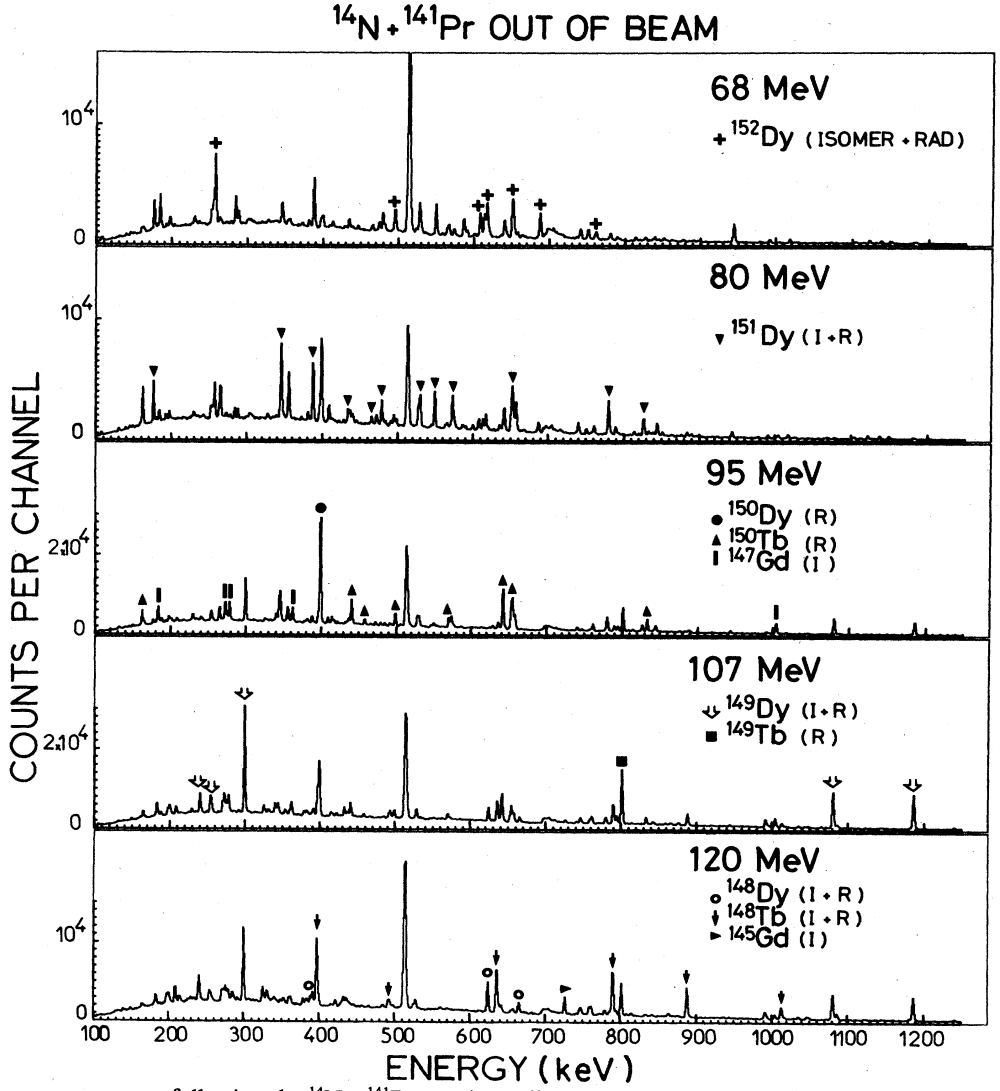

FIG. 2. Gamma-ray spectra following the $^{14}N+^{141}Pr$ reaction collected between the beam bursts in the nanosecond range.

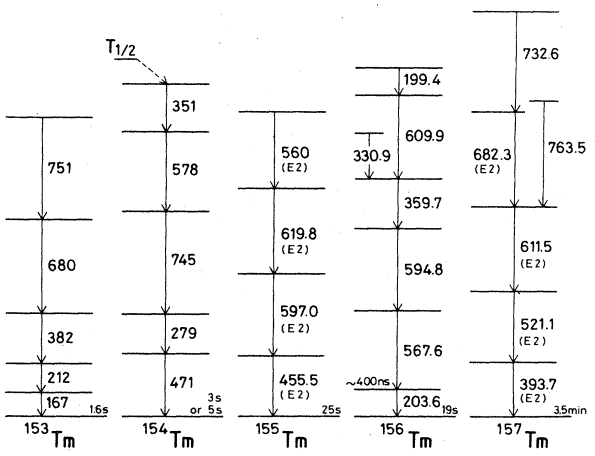

FIG. 3. Partial level schemes for $^{153-157}$Tm nuclei, excited in the ^{144}Sm(^{14}N,xn) and ^{147}Sm(^{14}N,xn) reactions at bombarding energies from 80 to 120 MeV. The gamma cascades were established from excitation functions, angular distributions (for ^{155}Tm and ^{157}Tm only), and prompt and delayed gamma-gamma coincidences. In ^{154}Tm the observed cascade is fed by a high spin isomeric state. Except for the ^{157}Tm nucleus, the order of transitions is only tentative.

produced residual nuclei.

In order to deduce the formation cross section from radioactivity data, the correction for the recoil of nuclei from the target was applied assuming full momentum transfer from the projectile to the compound system. Owing to thick targets employed in the present work, this correction was small, usually of the order of 10%. For the radioactive products having half-lives longer than or comparable with the time of measurement, the correction for the growth of activity was also made, assuming no beam variation during the irradiation of the target. The intensities per decay for radioactive gamma rays were taken from Refs. 29 and 30.

The cross sections determined from radioactive decay were particularly useful in the cases of some odd-odd nuclei, for which in-beam transitions are not well known or the ground state is fed by a number of weak cascades.

IV. EXPERIMENTAL RESULTS

A. Cross sections of heavy reaction residues

The complete set of the heavy residue production cross sections is presented in Tables II—V. Errors take into account uncertainties in the determination of the peak areas, in the correction factors described in the preceding section, and, in some cases, the ambiguities of line identification.

We estimate the absolute normalization error (not included in Tables II—V) as 20%. The relative errors between different systems and energies are, however, smaller due to the method of normalization, which does not depend on the target thickness and its homogeneity (see the Appendix for details).

For several bombardments only relative cross-section values were determined. In such cases the normalization factors were obtained by interpolation of the total observed cross section and/or the cross section for the target excitation measured for the same system at other energies (and assumed to vary smoothly with the bombarding energy).

For the cross sections of some products only the upper limits are given. These limits mean that a given product was looked for but could not be found with a good confidence level. In the following, the upper limit values are not taken into account in the data where the sum of the cross sections was of interest. The detection threshold for the individual gamma transitions varied with projectile energy. For the lowest bombarding energies, transitions of 1—2 mb were detected, whereas this limit was about 10 mb at higher energies.

In Fig. 4 the excitation functions for the formation of Dy(xn) and Tb(pxn) nuclei in the ^{14}N+^{141}Pr reaction and in Fig. 5 examples of mass and charge distributions are shown as an illustration of the data given in Tables II—V. At high bombarding energy the cross sections for $\Delta Z=1$ and $\Delta Z=2$ residues are as important as for the $\Delta Z=0$ ones in the reactions on ^{141}Pr and ^{147}Sm targets, and even more important in the reactions on the ^{144}Sm target. For systems which are more neutron-rich, the neutron evaporation dominates in the whole energy range studied.

A group of residues with $\Delta A\approx 12$ to 16 and $\Delta Z\approx 5$ to 7, well separated from complete fusion products, can be observed in Fig. 5. This group of "target neighboring" nuclei is systematically produced by the ^{14}N projectile and is almost unobserved (see Tables II—V) for the ^{12}C-induced reactions. Its whole cross section is attributed to reactions where only a small part of the projectile is transferred to the target. This cross section does not exceed 10% of the total observed cross section. In the following, the cross sections for residues of ΔZ greater than 4 are not included in the data where the evaporation from the compound nucleus is discussed.

The evolution of the total cross section observed with

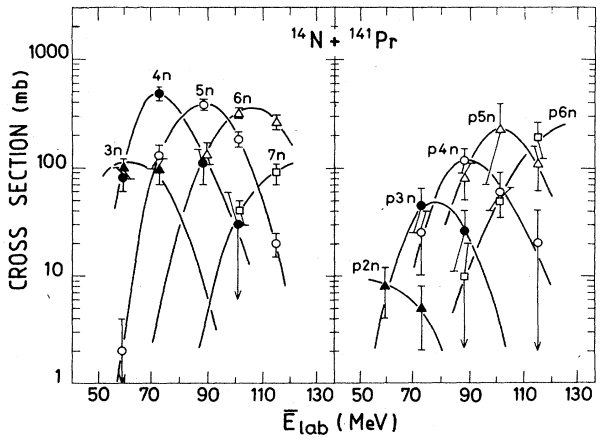

FIG. 4. Experimental excitation functions for the xn and pxn products observed in the ^{14}N+^{141}Pr reaction. The lines are drawn to guide the eye. Some experimental points, corresponding to small cross-section values having relatively big errors, are not shown explicitly, but are taken into account in the extension of the curves.

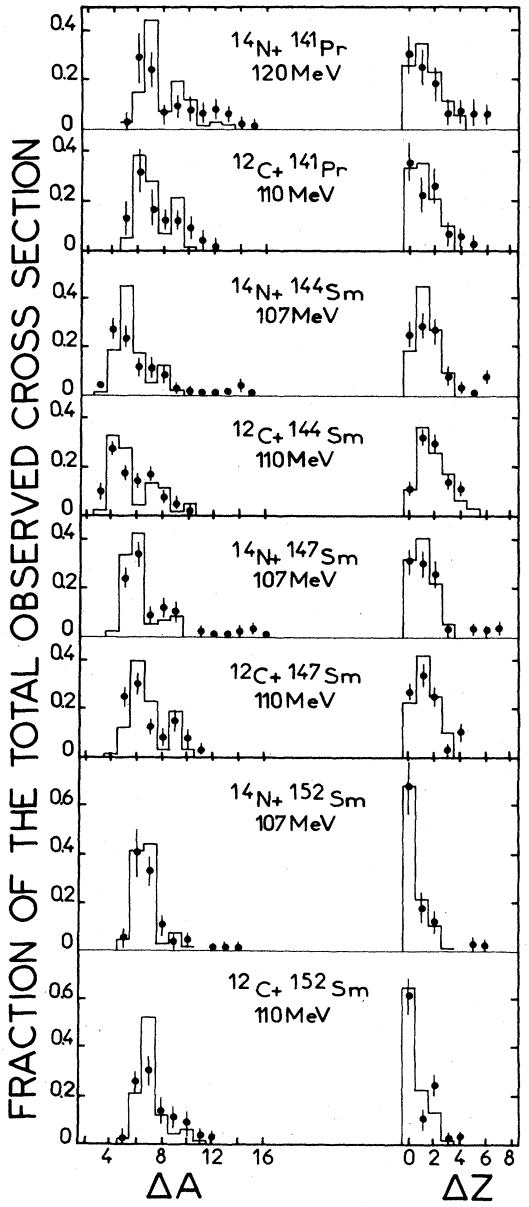

FIG. 5. Examples of mass and charge distribution of evaporation residues. The results of the evaporation code LANCELOT are given by the solid histogram.

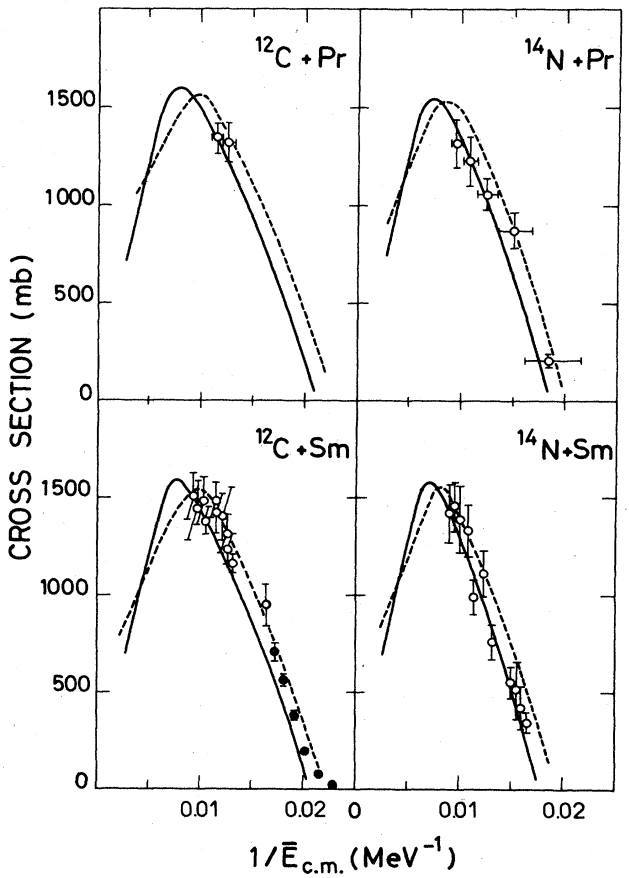

FIG. 6. The total observed cross section versus the inverse of the incident energy in the center of mass system. Solid lines represent the fusion cross-section calculations according to Ref. 32, dashed lines those according to Refs. 31 and 34. The closed points are taken from Ref. 7 for the ^{12}C+^{152}Sm reaction, open points from the present work (the data normalized by interpolation between other energies are not plotted). Horizontal bars shown for reactions on the ^{141}Pr target indicate the upper and lower limits set by the energy spread in the target.

the center of mass energy of the colliding nuclei, $E_{c.m.}$, is presented in Fig. 6. The calculated[31–34] fusion cross sections are shown by way of comparison. These calculations are discussed in Sec. V A.

B. Gamma-ray multiplicity

Gamma-ray multiplicity has been measured for a number of residues. This measurement clearly indicates the range of angular momentum we are dealing with and allows a comparison with the previous studies performed in this mass region.[5,35,36]

In order to convert the experimentally determined gamma-ray multiplicities $\langle M \rangle$ to the angular momentum $\langle l_m \rangle$ of states prior to gamma decay, the usual formula was employed:

$$\langle l_m \rangle = f(\langle M \rangle - k) + I_{g.s.} , \quad (1)$$

where f is the average angular momentum removed from the excited evaporation residue by the yrast gamma transition, k is the number of "statistical" gamma quanta which remove, on the average, a zero angular momentum, and $I_{g.s.}$ denotes the spin of the ground state in a given residue. Constant values $f=2$ and $k=4$ have been used according to Ref. 5.

In Fig. 7 we compare the average $\langle l_m \rangle$ for the xn fraction of the cross section, $\overline{\langle l_m \rangle}_{xn}$, with the average initial angular momentum of the compound nucleus, $\langle l_{CN} \rangle$, calculated from the classical trajectory model of Beck *et al.*[31] (as discussed in Sec. V A, this model reproduces the experimentally observed cross sections well).

Up to about 40$\hbar$, $\overline{\langle l_m \rangle}_{xn}$ well represents the initial angular momentum, while above 40$\hbar$ ($l_{max}=60\hbar$) a saturation occurs. This saturation was explained in Ref. 5 as the approach of the critical angular momentum for fission

TABLE II. Heavy residue cross sections given in millibarns. $\bar{E}_{lab}$ is the average projectile energy at half-thickness of the target; σ_{XK} is the calculated cross section for fluorescent K x rays in barns. The data corresponding to the σ_{XK} values marked with asterisks were normalized by interpolation from other energies (see the text).

Reaction	$^{12}C+^{144}Sm$				$^{12}C+^{147}Sm$			$^{12}C+^{150}Sm$	
$\bar{E}_{lab}$ (MeV)	73.5	81.9	90.3	102.5	85.2	93.4	105.8	85.2	105.8
σ_{XK} (b)	27.6*	37.5	49.2*	68.7	38.9	50.8	71.2	41.9	74.6
2n	26±4	17±4			<20				
3n	159±30	94±10	38±6		40±8	<30		31±15	
4n	115±20	166±18	120±15	30±9	215±39	84±32	<20	118±24	<24
5n		27±4	71±10	82±16	324±16	402±24	211±33	511±47	73±16
6n			16±10	45±25	11±5	84±16	159±16	181±39	367±41
7n						8±8	33±8	12±12	245±41
8n									57±12
9n									<8
p1n	14±6	18±6			<10				
p2n	162±22	95±19	20±6		16±16			<15	
p3n	170±15	264±18	230±20	106±16	80±23	12±12	<25	20±8	
p4n	17±6	90±14	233±16	260±16	154±31	221±32	155±24	79±50	16±16
p5n			29±10	91±25	18±6	141±28	286±57	31±15	94±33
p6n				5±5		<20	69±24	<15	87±24
p7n							<25		37±12
2p0n	12±10								
2p1n	33±15								
2p2n	12±12	8±8	3±3		<20				
2p3n	26±6	14±9	44±8	35±11	20±12		<25	<20	
2p4n	96±15	73±9	68±9	106±17	20±16	22±8	<10	24±12	<16
2p5n	44±10	110±8	137±14	124±9	122±16	92±16	81±12	79±15	33±16
2p6n	15±5	19±9	79±10	124±13	113±23	173±40	125±41	118±31	122±24
2p7n				30±30	<25	68±16	152±33	24±8	130±33
2p8n						<10	24±16	<12	57±12
2p9n									<24
3p3n	22±10	18±8							
3p4n	3±2	28±8	33±8	69±16	23±16	9±9		19±19	17±17
3p5n		9±4	38±10	84±7	23±12	26±8	<20		
3p6n			13±6	37±13	<10	12±12	24±16	<31	25±15
3p7n				<9		<10	20±20		12±12
3p8n							<20		
4p2n	11±11								
4p3n	7±7	8±8		<11					
4p4n	22±10	51±16	8±8	25±16	<20				<16
4p5n	26±4	35±3	28±5	38±4	51±23	57±24	51±24	<24	<41
4p6n	8±3	19±3	38±9	63±6	<25	48±48	63±33	47±24	57±30
4p7n			14±7	25±13		27±12	43±16	20±15	41±16
4p8n							<20	<24	16±16
4p9n									<20
Total	1000±58	1163±47	1260±47	1379±66	1230±75	1486±97	1496±107	1314±100	1486±112
Coulomb + inel								321±47	345±41

by the formed systems. A similar limitation of the evaporation residue cross section was recently observed at $l_{max}=35\hbar$ for the ^{200}Pb compound nucleus.[37]

The agreement of $\overline{\langle l_m \rangle_{xn}}$ with $\langle l_{CN} \rangle$ below $40\hbar$ does not cease even if the xn fraction does not account for the majority of the cross section (Fig. 8). This suggests that the neutron to charged particle evaporation ratio does not depend strongly on the CN angular momentum. However, our data should not be regarded as a decisive argument against the existence of such a dependence.[1] In the deexcitation of compound nuclei, where charged particles are being emitted with high probability, several dipole transitions are expected to occur in the yrast cascade for nuclei close to $N=82$ [this would make our simple calibration given by formula (1) untrue]. This effect may lead to an overestimate of $\overline{\langle l_m \rangle_{xn}}$ and may mask a possible enhancement of the charged particle emission from high angular momentum space.

TABLE III. Same as Table II.

Reaction	^{12}C+^{152}Sm				^{12}C+^{154}Sm		^{12}C+^{141}Pr			
$\bar{E}_{lab}$ (MeV)	65.5	85.2	93.4	105.8	88.0	108.0	77.4	85.5	93.8	106.1
σ_{XK} (b)		41.9	53.8	74.6	45.8	78.6	50.1*	66.0	84.5	117.0*
2n	<25				<15					
3n	80±40				200±100		36±13			
4n	550±70	50±20	<16		750±70	90±20	408±76	212±20	49±8	6±3
5n	230±60	500±100	161±40	40±20	200±70	480±80	212±35	482±70	403±37	142±13
6n	<15	450±50	604±56	270±40	<15	300±60		89±15	230±30	306±27
7n		30±15	145±24	450±100		<30				91±25
8n		<10	<16	170±30						
9n				<10						
p2n					<25		28±12			
p3n	20±20		<32		60±30	30±30	63±12	28±4		
p4n	<30	10±10	71±28	<30	30±20	80±40	64±18	152±31	102±11	57±10
p5n		28±15	69±32	60±30		50±20		30±5	146±15	162±13
p6n		15±15	24±16	35±20					23±8	121±13
p7n			<16	25±15						8±4
p8n				<20						
2p2n										
2p3n	<30						5±5	17±8		
2p4n	20±20				<20		45±6	19±6		21±6
2p5n	30±20	40±20	<32	<30	25±25		124±12	119±10	75±8	45±6
2p6n	<15	110±20	110±16	55±20	75±25	<30	20±12	87±24	128±23	122±13
2p7n		40±20	140±24	190±30	30±20	80±50			56±23	155±19
2p8n			32±32	130±30	<20	150±50			23±23	65±19
2p9n			<16	<20		40±20				
2p10n						<20				
3p4n		<30					7±3	8±8		
3p5n		<40		<60	10±10			12±12	19±19	49±6
3p6n		<40	25±25	<65					19±5	28±10
3p7n		<40		<40		50±50				23±3
3p8n				<60						
3p9n				<30						
4p4n			<16							
4p5n							23±6	12±12		
4p6n	<30	<30	40±25	<30	30±15	40±20	15±12	31±12	45±11	45±25
4p7n	17±17	40±15	<32	35±20	<20	<30		24±12	23±15	36±19
4p8n		<30	<24	30±30		40±20				
4p9n				20±20		<50				
5p6n										23±10
5p7n										13±10
Total	947±108	1313±123	1421±104	1510±135	1410±152	1430±148	1050±91	1322±90	1341±71	1518±64
Coulomb + inel	650±100	500±90	473±100	569±150						

C. Competition between neutron and charged particle emission

It was shown in Fig. 6 that the total observed cross section depends, for all the studied systems, mainly on the energy in the center of mass. The relative contribution of various exit channels to this total cross section depends strongly not only on the energy, but also on the system studied.

In Fig. 9 the relative importance of the reaction channels in which 0, 1, and 2 charge units are emitted is presented for the ^{12}C+^{144}Sm and ^{14}N+^{141}Pr reactions as a function of the excitation energy. A strong decrease of the xn channel with increasing energy is observed for both reactions. It is also evident from this figure that the excitation energy is not the unique parameter governing the relative contribution of various reaction channels. Charged particle emission also strongly depends on the "neutron deficiency" of the compound nucleus formed in

TABLE IV. Same as Table II.

Reaction	$^{14}N+^{144}Sm$			$^{14}N+^{147}Sm$				$^{14}N+^{150}Sm$			
$\bar{E}_{lab}$ (MeV)	66.5	83.0	96.0	73.0	88.5	101.0	114.5	72.0	88.0	100.5	114.0
σ_{XK} (b)	15.2	30.3	46.4	20.4	36.6*	53.7*	76.2	19.6	36.0	52.9	75.3
2n	13±5	5±5									
3n	126±30	70±40	20±20	70±25	<14			15±15	<20		
4n	75±15	150±50	180±40	250±60	107±3	<17		240±120	82±40	15±15	
5n	<5	25±10	53±20	10±10	213±43	153±35	30±30	140±50	330±50	120±20	16±16
6n		<5	<15	<5	72±28	190±46	190±30	15±15	300±50	470±100	180±80
7n						46±23	200±40		20±10	130±30	220±50
8n							<10			<10	45±15
9n											15±15
p1n	5±5	10±10									
p2n	45±15	50±20	20±20	20±10	<14						
p3n	31±10	100±40	58±20	84±30	57±28	<17		30±15	20±20	<15	
p4n	3±3	75±15	140±30	18±10	136±28	150±35	40±40	50±50	120±50	40±20	10±10
p5n	<5	10±10	65±15	<5	40±21	224±46	190±30	26±15	120±60	195±40	85±30
p6n			<5		14±14	12±12	174±40		10±10	100±25	150±50
p7n							20±20			<20	125±25
p8n											<10
2p2n			29±10	<5	<7						
2p3n	2±2	30±15	42±20								
2p4n	15±5	30±10	48±20	28±15	21±14	12±12	10±10	<10	<10	<10	<25
2p5n	10±3	77±15	100±30	30±20	36±36	58±23	105±25	10±10	10±10	10±10	<25
2p6n		11±3	45±10	8±8	104±36	151±46	70±30	<10	34±15	33±15	<50
2p7n		<5			<14	100±29	140±30		45±15	105±40	120±50
2p8n							32±20		4±4	44±20	200±50
2p9n										7±7	46±15
3p2n			<5								
3p3n	<3	<5	<10	<5	<14						
3p4n	<2	10±5	10±10	15±15	14±14		<20				
3p5n		60±20	40±20	<5	<21	<23	<20			10±10	
3p6n		5±5	25±5		<7	32±17	90±40			10±10	20±20
3p7n			<5			<23	10±10			15±15	90±30
3p8n										<15	10±10
4p4n			<15								
4p5n		<5	<10	<10			<10				
4p6n		11±3	17±5	<10		<23	<20				
4p7n		<5	13±5				28±28				
4p8n							<20				25±25
4p9n											<20
5p5n	<2								<10	<10	<10
5p6n	<5	<8	<10	<5	7±7	23±23	10±10		<15	<15	<15
5p7n	1±1	3±3	5±5	<5	7±7	9±9	15±15		<10	<15	
5p8n		<2	<5		7±7	12±12	10±10			<20	<20
5p9n							<10				
6p6n	5±3	6±3	10±10		<14		<10	3±3	<10		
6p7n	10±5	15±10	16±10	5±5	14±14	<23	<10	5±5	10±10	10±10	15±15
6p8n	2±2	10±10	46±20	<5	17±9	23±17	25±25		10±10	10±10	15±15
6p9n			5±5	<5	7±7	10±10	18±18			10±10	15±15
6p10n					<7		6±6				
7p8n	2±2			15±15	21±21	35±35	30±30	<20	<20		
7p9n				<5	<7	12±12	15±15				
Total	345±40	763±89	987±86	553±81	894±98	1252±117	1458±126	534±143	1115±119	1334±131	1402±147
Coulomb + inel	23±5	27±7	25±5	72±15	85±36	87±17	93±30	558±50	533±50	493±50	440±70

TABLE V. Same as Table II.

Reaction	^{14}N + ^{152}Sm				^{14}N + ^{141}Pr				
E_{lab} (MeV)	71.0	87.0	100.0	113.5	59.5	72.5	88.0	101.0	114.0
σ_{XK} (b)	18.8	34.7*	52.1*	74.4	16.9	31.4	56.6	84.1	117.0
2n					<5	<15			
3n	15±15				100±20	95±25	<15		
4n	130±30	34±17			80±20	485±70	110±40	30±30	
5n	230±100	271±57	63±31	<30	2±2	130±30	380±40	185±30	20±15
6n	30±15	283±113	350±125	120±60		<10	120±25	320±30	265±40
7n		68±34	375±63	320±80			<5	40±10	90±20
8n		6±6	50±25	340±80					20±20
9n				30±15					
p1n					<3				
p2n					8±4	5±3			
p3n	15±15				<6	45±20	26±15	<10	
p4n	25±25	<34	<25		<3	25±15	120±30	60±30	20±20
p5n	<10	90±45	150±50	<20		<15	80±30	220±100	110±50
p6n		<23	31±31	180±60			10±10	50±15	190±70
p7n			38±19	170±70					20±10
p8n				25±25					
2p3n					<4				
2p4n					15±10	20±20	<30		<20
2p5n		<17			3±3	50±25	60±20	30±30	30±30
2p6n		34±34	38±19	15±15		15±10	80±20	90±20	30±10
2p7n		28±28	50±25	40±20			25±15	110±20	65±25
2p8n		<6	56±38	95±30			<5	10±10	70±20
2p9n				60±30					50±30
2p10n				<10					
3p4n					<1				
3p5n					<2	<10	<15	<10	<10
3p6n						<10	10±10	30±30	50±20
3p7n							<10	<10	30±10
3p8n									5±5
4p5n					<3	<15	<10		<10
4p6n					<2	3±3	13±5	<15	10±10
4p7n						1±1	11±5	30±10	20±10
4p8n							8±5	20±10	40±20
4p9n							<10	<15	20±10
5p5n		<11							
5p6n							<15		
5p7n			10±10	10±10			<15	<30	15±15
5p8n			10±10	10±10			<15	<15	30±20
5p9n				<15					20±20
5p10n									10±10
6p6n	<10	<17							<20
6p7n	<20								50±20
6p8n		15±15		10±10					25±25
6p9n				<20					10±10
6p10n									<15
Total	445±110	829±147	1221±166	1425±169	208±30	874±91	1053±85	1225±129	1315±125
Coulomb + inel	1320±220	1322±147	1350±125	910±100	26±4	43±9	43±6	43±5	32±16

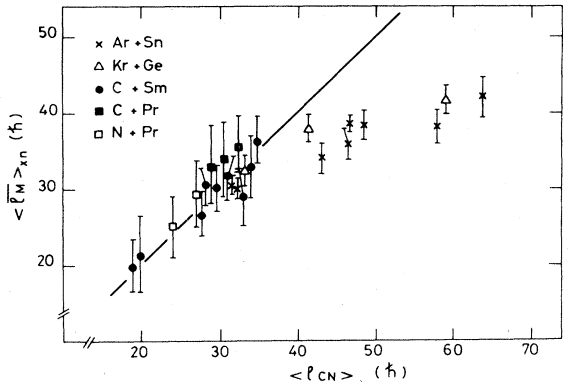

FIG. 7. Comparison of the angular momentum of xn residues $\overline{\langle l_m \rangle_{xn}}$ with the average CN angular momentum $\langle l_{CN} \rangle$ predicted according to Refs. 31 and 34. The data for the Ar- and Kr-induced reactions are taken from Ref. 5.

the reaction. For a given excitation energy the sum of the xn cross sections decreases linearly (Fig. 10) with the distance of the CN from the stability line, $(N/Z)_{CN}-(N/Z)_{stab}$ (the total cross section does not show such a dependence). The $(N/Z)_{stab}$ value is defined as the abundance-weighted average N/Z value of the stable isotopes. The same effect can be seen in Fig. 11, where the fraction of the observed cross section for a given emitted charge ΔZ is plotted for two values of the excitation energy of the compound nuclei.

The decrease of the xn products cross section far from the stability line was previously discussed in Ref. 3. In that work an effective proton binding energy including the Coulomb barrier was determined in a number of reactions, and a simple relationship between the proton to neutron evaporation rates, binding energies, and nuclear temperature was established. In the investigated mass region the data point to an even more serious limitation of the xn products cross section than that predicted by the simple formulae of Ref. 3. For instance, for the most

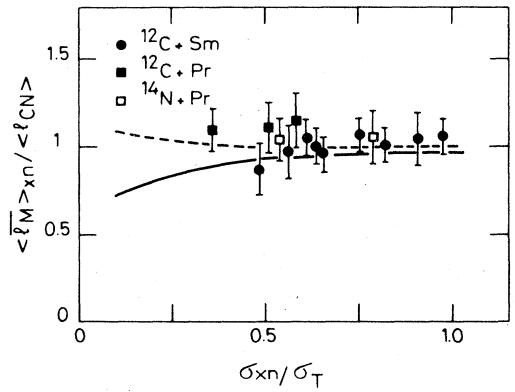

FIG. 8. Ratio of the average angular momentum of xn residues to the average angular momentum of CN as a function of the fraction of the observed cross section, leading to the xn channel. $\langle l_{CN} \rangle$ has been calculated as in Fig. 7. The lines correspond to the evaporation calculations by ALICE (dashed line) and LANCELOT (solid line). See Ref. 16 for details.

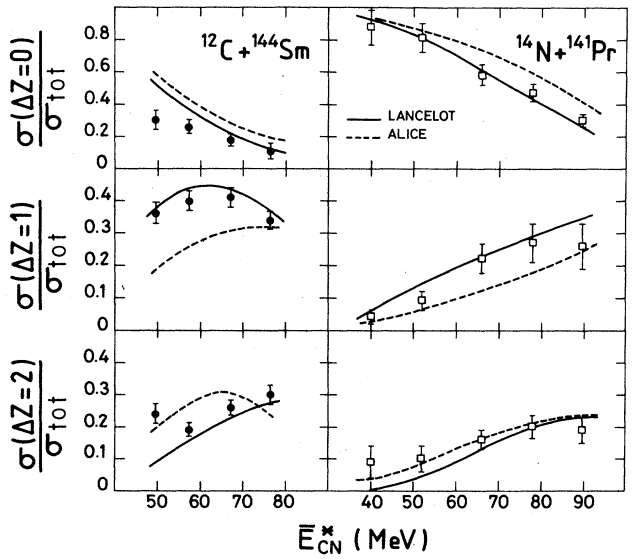

FIG. 9. Fractions of the observed cross sections for different evaporated charged ΔZ as a function of the excitation energy. The lines correspond to the calculations by ALICE (dashed lines) and LANCELOT (solid lines).

neutron-deficient systems studied (reactions on ^{144}Sm), at $E^* \approx 78$ MeV these formulae attribute about 60% of the cross section to xn products, whereas the measured value is only about 10%.

D. Average removed charge

The competition between neutron and charged particle emission can also be characterized by the average removed

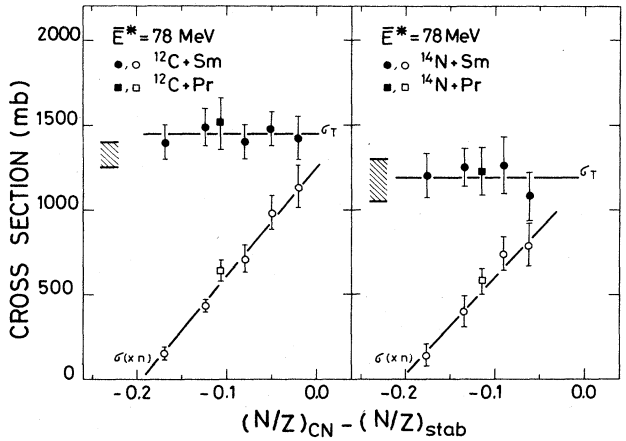

FIG. 10. Total observed cross sections and xn cross sections for different reactions leading to compound nuclei at 78 MeV excitation energy as a function of the distance of the CN from the stability line (see the text). The points originate from interpolation (or extrapolation in some cases) of the experimental results, measured at adjoining energies. The hatched area indicates the range of cross sections predicted by classical trajectory calculations for different targets (Fig. 6) (the spread is mainly due to the difference in the reaction Q values). The solid lines are drawn to guide the eye.

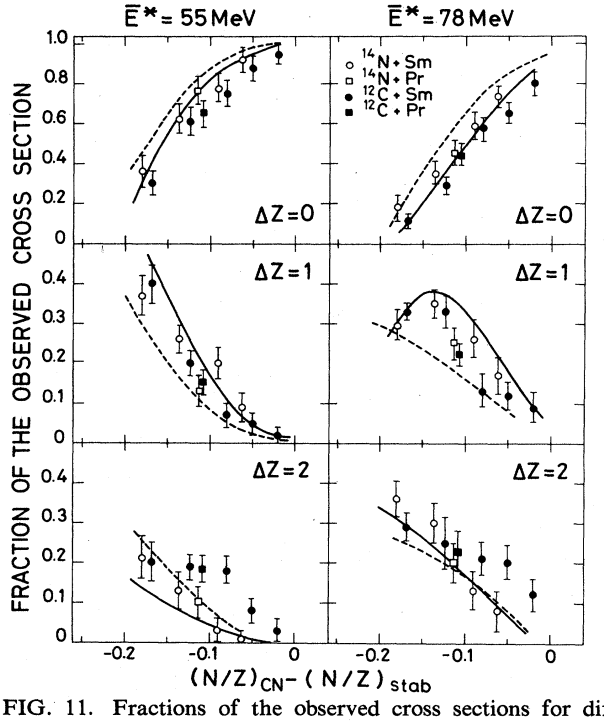

FIG. 11. Fractions of the observed cross sections for different evaporated charges ΔZ as a function of the distance of the CN from the stability line for 55 and 78 MeV excitation energies. Only $\Delta Z = 0$, 1, 2, 3, and 4 channels were taken into account when calculating the average. The solid lines correspond to the LANCELOT and the dashed lines to the ALICE calculations.

charge, $\overline{\Delta Z}$, defined as the cross-section weighted difference between the charge of the compound nucleus and the charges of the residual products. Figure 12 presents $\overline{\Delta Z}$ as a function of the excitation energy for several investigated systems.

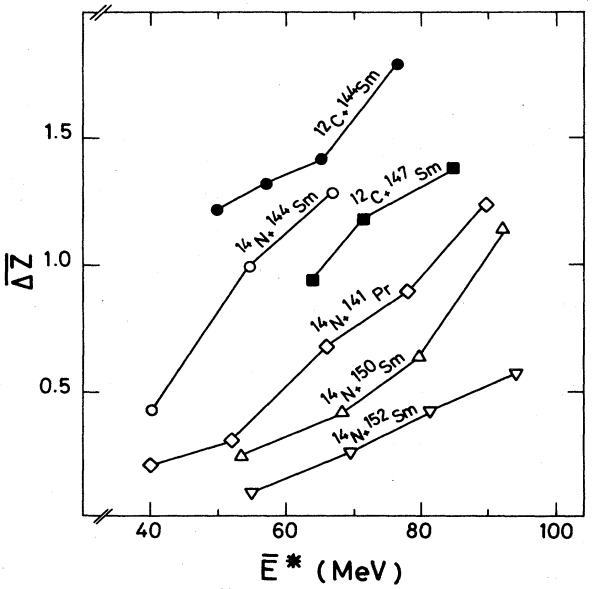

FIG. 12. Average difference between the compound and residual nuclei charges $\overline{\Delta Z}$ (determined from $\Delta Z = 0$, 1, 2, 3, and 4 channels only) as a function of the CN excitation energy.

In the calculation of $\overline{\Delta Z}$ the average was taken over $\Delta Z = 0$, 1, 2, 3, and 4 channels. As discussed above (Sec. IV A), the $\Delta Z = 5$, 6, and 7 products observed in ^{14}N-induced reactions, attributed to a process other than evaporation from the CN, are not included in this calculation.

For a given target and projectile, $\overline{\Delta Z}$ increases with energy, as well as, for different systems, with the distance of the CN from the stability line. These effects are illustrated in Fig. 13 for two selected CN excitation energies.

The average removed charge for the ^{12}C-induced reactions systematically exceeds the values observed in the ^{14}N-induced reactions. This difference, further discussed in Sec. V D, may indicate a stronger contribution of the incomplete fusion process to the formation of $1 \leq \Delta Z \leq 4$ products in the case of the ^{12}C projectile.

The data from Ref. 4 concerning the ^{32}S + Sn reactions are plotted in Fig. 13 for comparison. The average evaporated charge for the ^{32}S data does not show any significant difference from the corresponding values for the ^{14}N-induced reactions. The maximum CN angular momentum populated in the ^{32}S-induced reaction, estimated from the sharp cutoff approximation, is about 60$\hbar$. However, the l_{max} value calculated from the evaporation residue cross section is only slightly higher for the ^{32}S-induced reactions than for the ^{14}N projectile (50$\hbar$ and 48$\hbar$, respectively, for 78 MeV E^*).

E. Average removed mass

For a given excitation energy the average difference between the CN mass and the residual product masses, $\overline{\Delta A}$, does not depend, within 5%, on the target-projectile combination. This is illustrated for two selected excitation energies in Fig. 13. In the investigated energy range $\overline{\Delta A}$ changes linearly with E^*; the same relationship holds for all the systems studied (Fig. 14). On the average, an in-

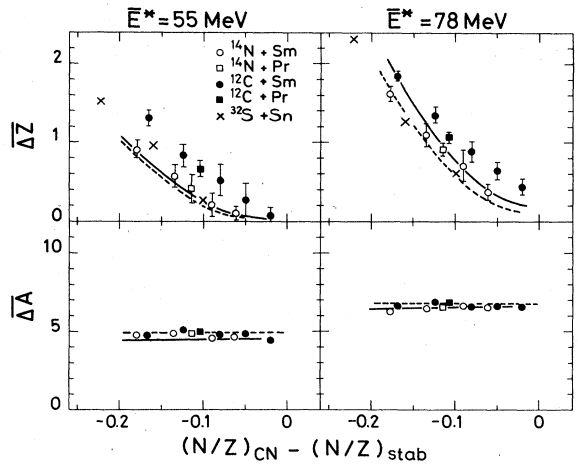

FIG. 13. Average charge and mass removed from the compound nucleus at 55 and 78 MeV excitation energy as a function of the distance of the CN from the stability line. The data for the ^{32}S-induced reactions are taken from Ref. 4. The calculations of ALICE and LANCELOT for ^{12}C- and ^{14}N-induced reactions are represented by dashed and solid lines, respectively.

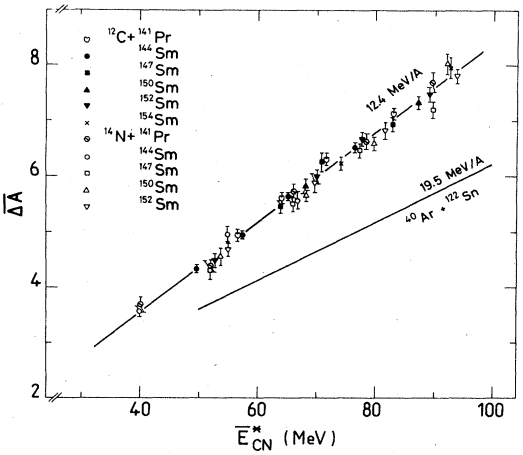

FIG. 14. Average evaporated mass as a function of the CN excitation energy. Only $\Delta Z=0$, 1, 2, 3, and 4 channels were taken into account when calculating the average. The line for the ^{40}Ar+^{122}Sn reaction is taken from Ref. 38.

crease of 12.4 MeV of the CN excitation energy is needed to evaporate one mass unit in ^{12}C- and ^{14}N-induced reactions.

The variation of the average evaporated mass with excitation energy was previously reported[38] for ^{40}Ar-induced reactions leading to the same compound nuclei as those investigated in the present work. A strong difference of $\overline{\Delta A}$ and its slope vs E^* is observed between ^{12}C or ^{14}N and ^{40}Ar projectiles (Fig. 14). This effect, discussed in Sec. V B, is connected with the differences in the angular momentum brought into the compound nucleus.

The independence of $\overline{\Delta A}$ of the system studied in ^{12}C- and ^{14}N-induced reactions is valid only if the average is deduced from the whole set of evaporation products. This is illustrated in Fig. 15, where the average removed mass is presented separately for the xn, αxn, and $2\alpha x$n reaction channels [$(\overline{\Delta A})_{xn}$, $(\overline{\Delta A})_{\alpha xn}$, and $(\overline{\Delta A})_{2\alpha xn}$, respectively].

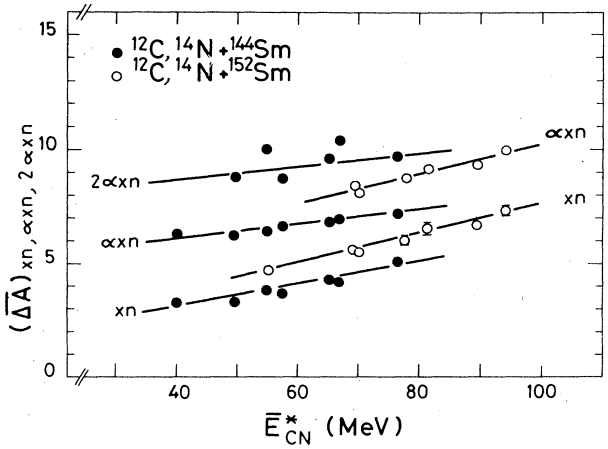

FIG. 15. Average evaporated mass for xn, αxn, and $2\alpha x$n channels for reactions on the ^{144}Sm and ^{152}Sm targets as a function of the CN excitation energy. The pxn channels follow the same dependence as the xn data. The lines are drawn to guide the eye.

A clear difference between reactions leading to the formation of neutron-rich CN (^{164}Er, ^{166}Tm) and those corresponding to neutron-deficient ones (^{156}Er, ^{158}Tm) is observed. Indeed, for neutron-deficient systems the emission of a neutron is associated with an energy loss higher than that for neutron-rich systems (due to the higher neutron binding energy of the former). In consequence, for a given excitation energy the average number of emitted neutrons is smaller for the deficient systems.

The decrease of $(\overline{\Delta A})_{xn}$ for neutron-deficient CN is, however, much stronger than expected from the simple difference between the binding energies in neutron-rich and neutron-deficient nuclei. In Figs. 16 and 17 the $(\overline{\Delta A})_{xn}$ values are plotted against the average energy transmitted by the CN to the evaporated neutrons and to the associated gamma rays, $\langle E^{n}_{kin}+E^{tot}_{\gamma}\rangle$, given by

$$\langle E^{n}_{kin}+E^{tot}_{\gamma}\rangle = E_{c.m.}+\langle Q_{gg}\rangle \ , \tag{2}$$

where Q_{gg} can be found from the initial and final masses:

$$Q_{gg}=M_A+M_{HI}-M_B-xM_n \ , \tag{3}$$

and $\langle Q_{gg}\rangle$ obtained by averaging over all xn channels [in expression (2) we neglect the kinetic energy of the evaporation residue in the c.m. system]. This procedure permits us to subtract the neutron binding energies from the CN excitation energy.

It can be seen from Fig. 16 that, to evaporate, for example, five neutrons, the system transmits to these neutrons and to the associated gamma rays about 22 MeV energy in the ^{12}C+^{152}Sm reaction and about 30 MeV in the case of the ^{12}C+^{144}Sm reaction. Similarly, if we compare the

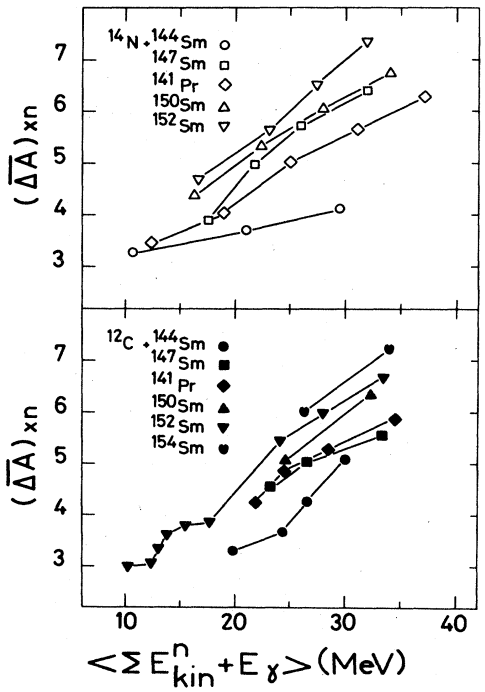

FIG. 16. Average number of evaporated neutrons in the (^{12}C,xn) and (^{14}N,xn) reactions as a function of their average kinetic energy plus the energy of emitted gamma rays.

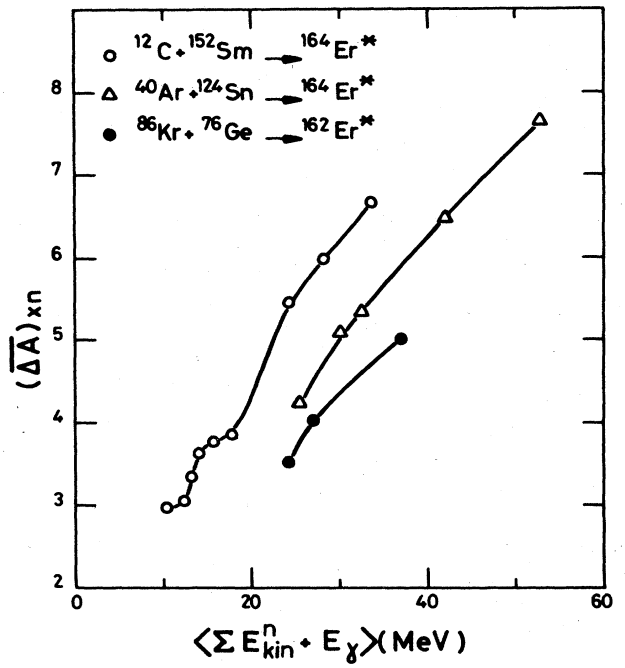

FIG. 17. The same as in Fig. 16, but for the ^{12}C-, ^{40}Ar-, and ^{86}Kr-induced reactions. The data for Ar and Kr were taken from Ref. 5.

^{12}C-, ^{40}Ar-, and ^{86}Kr-induced reactions (Fig. 17) we see also an important difference in $\langle E^{n}_{kin} + E^{tot}_{\gamma} \rangle$, required for the evaporation of a given average number of neutrons. The observed effects are also discussed in Sec. V B.

V. DISCUSSION

A. Total observed cross sections

The observed total cross sections have been presented in Fig. 6. The complete fusion cross sections, calculated according to two classical trajectory models of Beck *et al.*[31] and of Birkelund *et al.*,[32] are also shown for comparison. The model of Ref. 31 was employed with the following modifications:[34] (i) the liquid drop plus proximity potential was replaced by the folding potential;[33] (ii) the neck degree of freedom was introduced instead of "blowing up" the radii of the colliding nuclei, which means that the extra nuclear matter from the overlapping region goes into the neck which smoothly joins two spheres. The results of calculations are not very sensitive to the target neutron number, therefore one theoretical curve is representative for the different Sm isotopes.

The experimental cross sections, which approximately follow a linear dependence on $1/E_{c.m.}$, are fairly well reproduced by the calculations. This is consistent with the fact that the main part of the observed cross section results from the complete fusion process when the contribution of other reaction mechanisms does not exceed 10% (see Sec. V D).

As the major part of the fusion cross section was detected in the present investigation, the previously discussed competition of various reaction channels and average numbers represents, with a good approximation, the evaporation characteristics of the compound nucleus. Their comparison with the evaporation models is also justified (cf. Sec. V C).

B. Influence of angular momentum on the average number of emitted particles

The differences between the average $\overline{\Delta A}$ or $(\overline{\Delta A})_{xn}$ for light and heavy projectiles (Figs. 14 and 17) and $(\overline{\Delta A})_{xn}$ for light and heavy Sm targets (Fig. 16) can be attributed to the angular momentum effects. It may be assumed that $\overline{\Delta A}$ or $(\overline{\Delta A})_{xn}$ is proportional to E_{th}, the average thermal energy of a CN above the yrast line:

$$E_{th} = E^{*}_{CN} - \overline{E}_{y} - \overline{E}_{s} = E^{*}_{CN} - E^{tot}_{\gamma} , \quad (4)$$

where $\overline{E}_{y}$ is the average energy of the yrast gamma-ray cascade. $\overline{E}_{s}$ represents the average energy of the statistical gammas or, in other words, the average difference between the entry and yrast lines. Up to the limit of evaporation residue production, set by fission, $\overline{E}_{y}$ is an increasing function of $\langle l_{CN} \rangle$. Therefore, for a given E^{*}_{CN} a lower value of $\overline{\Delta A}$ [or $(\overline{\Delta A})_{xn}$] may be expected for higher $\langle l_{CN} \rangle$. This is observed indeed in Fig. 14. The different slopes of $\overline{\Delta A}$ vs E^{*}_{CN} for light and heavy projectiles can be explained by the faster increase of $\langle l_{CN} \rangle$ with E^{*}_{CN} for ^{40}Ar in comparison with ^{12}C or ^{14}N. The results presented in Fig. 17 can be explained along the same lines.

The difference in $(\overline{\Delta A})_{xn}$ between the light and heavy Sm targets (Fig. 16) is due to the fact that the light Sm targets require more initial energy to emit a given number of neutrons. Evidently, for the same projectile one cannot bring to the system more energy without an increase in its angular momentum and, consequently, E^{tot}_{γ}. In this way, although neutron binding energies are eliminated in the abscissa of Fig. 16, their effect still remains through the increased E^{tot}_{γ} for neutron-deficient systems.

The effects described are connected with the production of strongly neutron-deficient, highly rotating nuclei and are important in the medium-heavy mass region. On the contrary, for light systems the angular momenta involved are smaller and the steep increase of the charged particle emission prevents the production of nuclei far off the stability line. As was shown in Ref. 39, in such a case the number of evaporated neutrons follows a unique dependence on E^{*}_{CN} for all systems. On the other hand, for very heavy systems the excitation energy and the angular momenta leading to evaporation residues are strongly limited by the fission.

C. Statistical model calculations

The experimental results described in Sec. IV were compared with more detailed calculations of the evaporation model involving two different computer codes, ALICE of Blann[12,13] and LANCELOT of Cole.[14–16] The range of the LANCELOT code, originally performing calculations in the $A \lesssim 44$ region, has been extended up to $A \simeq 200$.[16] The main difference between these two codes consists in the treatment of the angular momentum in the particle eva-

poration process. In ALICE, the *s*-wave approximation is used, whereas in LANCELOT the change of the angular momentum due to particle emission is taken into account.

Liquid drop masses of Myers-Swiatecki (Lysekil) with shell but no pairing corrections were used, and a liquid drop moment of inertia was chosen in both cases. Neutron, proton, and alpha particle emission were taken into account, whereas the deuteron emission was assumed to be unimportant (see also Ref. 40). The fission competition was neglected: the data from Ref. 41 show that the fission cross section in the investigated mass and angular momentum range is small, of the order of 10 mb. The initial spin distribution of the compound nucleus was taken from the experimental fusion cross section as described in Ref. 15.

Both codes use the level densities in the version proposed by Lang.[42] However, in order to speed up the calculations, LANCELOT parametrizes the state densities with a given projection M of angular momentum, instead of level densities. In the original version of the code, the Lang formula with the parameters given by Gilbert and Cameron[43] was used at excitation energies above 15 MeV. We used the Lang formula in the whole energy range. The level density parameter a was set equal to $A/8$ in both codes. The ratio of the level densities used in ALICE to those generated by LANCELOT from state densities remains then approximately constant with the spin, excitation energy, and neutron and proton numbers of the studied nuclei. We estimate that the differences in the relative cross sections of the evaporation residues, due to the use of ALICE or LANCELOT level densities, are smaller than 5%.

The gamma-ray competition is included in LANCELOT following Grover and Gilat formulae for the $l=1$ and $l=2$ transitions.[44] In the ALICE code the deexcitation by gamma-ray emission is allowed only when the excitation energy above the yrast energy is lower than the effective binding energy of the particles (Coulomb barrier included). Table VI gives the values of gamma strengths and the optical model parameters used in LANCELOT calculations.

In Figs. 5, 8, 9, 11, 13, and 18 the experimental data are compared with calculations. Reasonable agreement between calculations and experiment is obtained. A slightly better fit to the experimental data is obtained with the LANCELOT code, but the use of the *s*-wave approximation does not seem to notably influence the calculations in these mass and angular momentum ranges.

In both calculations the average evaporated charge as a function of the distance of the CN from the stability line (Fig. 13) does not depend on the incident projectile. The experimentally observed difference between $\overline{\Delta Z}$ for ^{12}C and ^{14}N is not reproduced.

TABLE VI. Optical model parameters and multipole gamma strengths used in the LANCELOT code. The meaning of symbols used is the same as in Ref. 15. The values of V_0, R_0 and a were taken from Ref. 45. The ϵ_1 and ϵ_2 values were fitted to reproduce $\overline{\Delta A}$, whereas the ratio ϵ_1/ϵ_2 was kept constant.

Particle	V_0 (MeV)	R_0 (fm)	a (fm)
n	44.0	1.25	0.65
p	55.0	1.25	0.68
α	60.0	1.30	0.60
$\gamma(l=1)$		$\epsilon_1=5\times10^{-6}$	
$\gamma(l=2)$		$\epsilon_2=1\times10^{-7}$	

D. Processes other than complete fusion

As was indicated in Sec. IV, there are two bits of evidence for the existence of processes other than complete fusion from the cross-section data. Firstly, the population of channels with $\Delta Z>4$ is clearly observed in the ^{14}N-induced reactions, while it is almost nonexistent in the case of the ^{12}C projectile (Fig. 5). Statistical model calculations described in the preceding subsection do not predict any such extension of light particle evaporation leading to target-neighboring residues. Secondly, for the same "neutron deficiency" of the CN, the average ΔZ values for the ^{12}C-induced reactions systematically exceed those observed for the ^{14}N and ^{32}S projectiles (see Fig. 13), indicating an enhancement of $1\leq\Delta Z\leq4$ channels for the

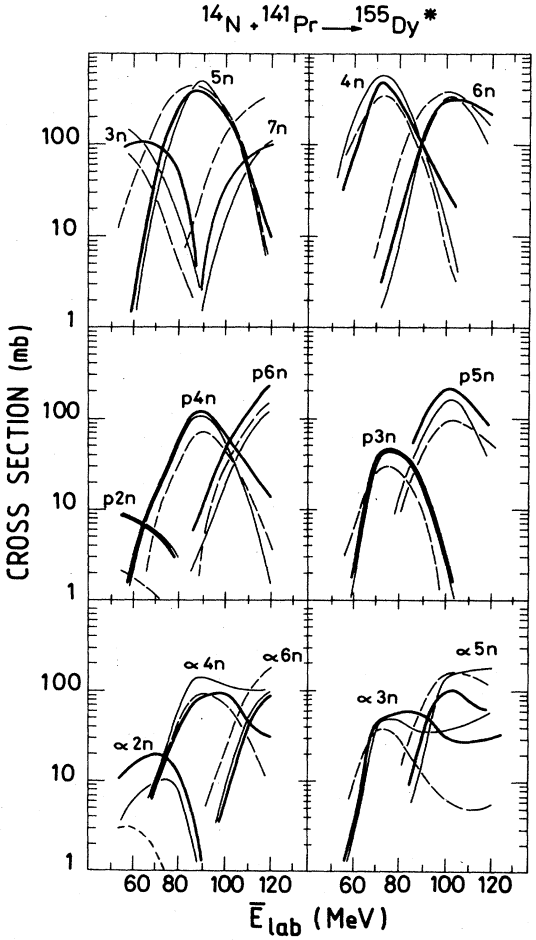

FIG. 18. Experimental excitation functions (thick solid lines) compared with the predictions of evaporation codes (ALICE—dashed lines, LANCELOT—thin solid lines). The experimental errors are indicated in Fig. 4. The calculated excitation functions were corrected for the spread of the beam energy in the target.

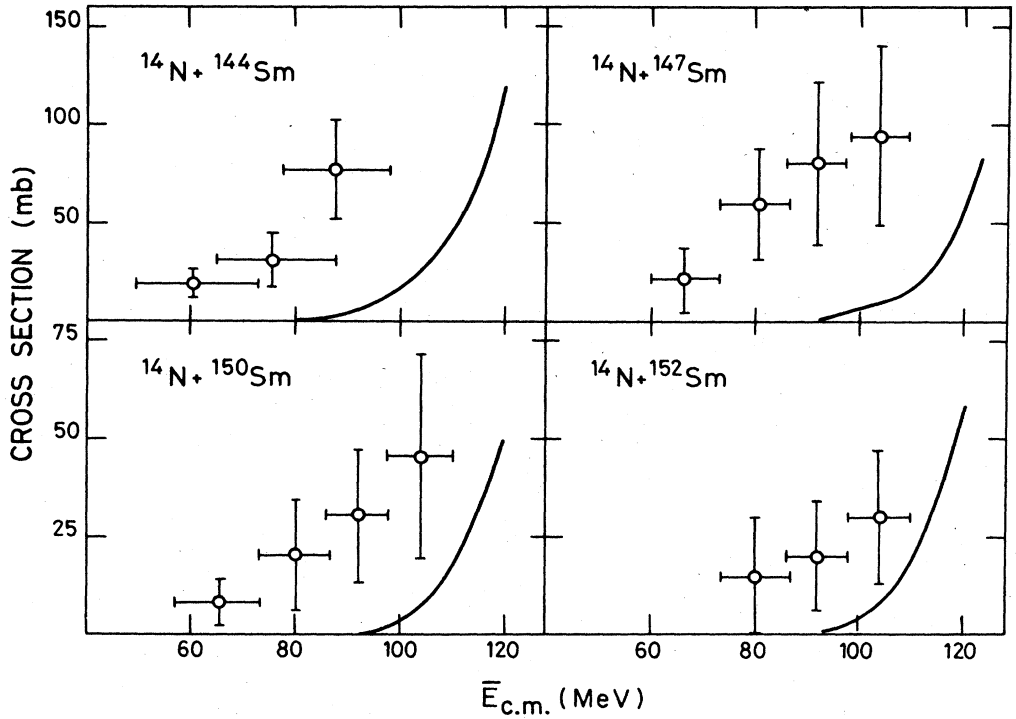

FIG. 19. Cross sections corresponding to the production of the target neighboring Gd, Eu, and Sm isotopes in the ^{14}N + Sm reactions as a function of the average c.m. bombarding energy. The horizontal bars indicate the upper and lower limits set by the energy spread in the target. The "sum-rule" model predictions for the cross sections of all binary processes leading to the transfer of 0, 1, and 2 charges to the target are shown by solid lines.

^{12}C projectile. This enhancement is mainly due to the $\Delta Z=2$ and $\Delta Z=4$ channels (see Figs. 5 and 11). Again, the statistical model calculations do not predict any drastic difference between the ^{14}N and ^{12}C projectiles in charge evaporation.

It was assumed that the processes which cannot be accounted for by the fusion evaporation model have as origin the incomplete fusion mechanism. To estimate the contribution of this mechanism, calculations were performed by means of the "sum-rule" model of Wilczynski *et al.*[46] for complete and incomplete fusion competition in the entrance channel. In these calculations the same set of parameters as in Ref. 46 was used [$T=3.5$ MeV, $\Delta l=1.7\hbar$, $R_c/(A_1^{1/3}+A_2^{1/3})=1.5$ fm].

The results of these calculations indicate that the incomplete fusion cross section does not exceed 10% of the reaction cross section in the considered energy range. The differences between the ^{12}C- and ^{14}N-induced reactions show up in the calculations. However, this difference is not strong enough to account for the $\overline{\Delta Z}$ differences observed experimentally. Similarly, the transfer of small fragments of the projectile to the target (n,p,d,t) is well predicted to be more pronounced for ^{14}N, but the observed cross sections for Gd, Eu, and Sm nuclei, produced in the ^{14}N+Sm reactions, strongly exceed the predictions of the calculations (Fig. 19).

VI. SUMMARY AND CONCLUSIONS

The extensive study of the formation of compound nuclei and their decay was performed in the $A\approx 160$ mass region for a large domain of excitation energies (40—100 MeV), angular momenta (up to 55$\hbar$), and for compound systems differing by as much as ten neutrons. The excitation energy, angular momentum, and neutron excess were shown to be the main factors governing the CN decay.

Comparison of the measured cross sections with model calculations indicates that the major part of the fusion cross section was detected by the experimental method employed. Therefore the observed trends in neutron and charged particle emission are representative for the compound nucleus decay.

The emission rate of charged particles was found to be strongly dependent on the excitation energy of the compound nucleus and its distance from the beta stability line. For the lightest system studied, at 80 MeV excitation energy, about 90% of the compound nucleus decay takes place by evaporation of at least one charged particle. The influence of the angular momentum on the charge evaporation was sought but could not be established.

The average mass emitted from the compound systems formed in the ^{12}C- and ^{14}N-induced reactions was found to be independent of the distance of the CN from the stability line (within 5%). In the energy range investigated, $\overline{\Delta A}$ increases linearly with the CN excitation energy. The comparison with heavier projectile data shows a strong influence of the angular momentum on the absolute value of $\overline{\Delta A}$ and its increase with E^*_{CN}. Angular momentum effects are also observed on the average number of emitted neutrons in the (xn) reaction channel.

The evaporation calculations reproduce quite well the

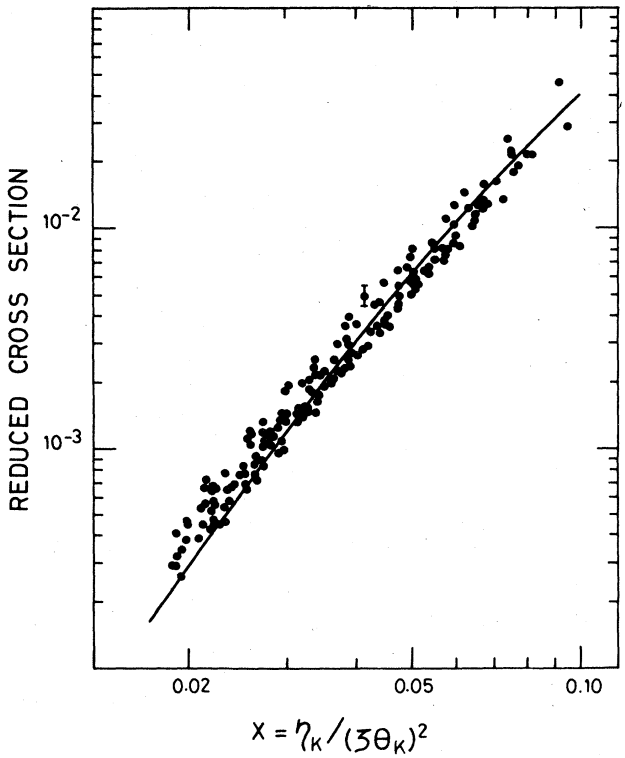

FIG. 20. *K*-shell ionization cross sections for target elements with $37 < Z < 57$ and ^{12}C, ^{14}N, and ^{16}O projectiles in universal representation (see the text). The experimental data are taken from Refs. 49—51. The energies of ions used in the present work correspond to X parameter values in the range 0.05—0.10.

average properties of the experimental results, in particular the strong charged particle emission from the neutron-deficient compound nuclei. Comparison of two computer codes shows that, in the angular momentum and mass ranges investigated, the "*s*-wave" approximation for particle evaporation does not strongly influence the calculated distributions of the evaporation residues.

In conclusion, for the mass region and the energy range studied, the statistical model (complete fusion plus evaporation process) satisfactorily accounts for the main features observed.

Nevertheless, a small part of the observed cross section originates from processes other than the complete fusion, even at relatively low bombarding energy. The calculations performed in the hypothesis of binary reactions (using the "sum-rule" model) do not quantitatively reproduce the observed effects. In particular the cross sections for the target neighboring residues are strongly underestimated. This point would need further study, including gamma particle coincidences and experiments at higher bombarding energies where the processes involving incomplete mass transfer are more important. The extension of the present investigation up to 30 MeV/u beam energy is in progress.[47]

ACKNOWLEDGMENTS

We would like to acknowledge Dr. J. Błocki, Dr. A. J. Cole, and Prof. J. Wilczyński for stimulating discussions. We are indebted to Dr. M. Zielinska-Pfabe for performing a part of the classical trajectory calculations. We also thank Prof. M. Moszynski and Dr. Z. Preibisz for the participation in the early stage of this work. Mr. G. Margotton is acknowledged for the technical assistance during the experiments, and the ISN cyclotron staff is acknowledged for efficiency in providing the beams. One of us (R.K.) would like to thank the IN2P3 and ISN for their hospitality. This work was carried out under the IN2P3-Warsaw University cooperation agreement.

APPENDIX

The normalization method consisting of simultaneous measurement of K x-ray and gamma-ray intensities was previously employed for lighter ions,[48,8] where the K-shell ionization cross sections are relatively well known or can be reliably calculated. In order to test whether the calculations may give reliable K-shell ionization cross sections for heavier projectiles, the available experimental data from Refs. 49—51 were compared with the calculated cross sections. Figure 20 shows these data in a universal representation in which the reduced cross sections are plotted against the reduced bombarding energy.

The long range Coulomb interactions between the target K electron and the projectile were taken into account in the calculations. The so-called "Pauli excitation effect," due to the overlapping of the target and projectile K shells, was neglected (this effect is negligible for systems where $Z_t \gg Z_p$.).

The calculations were carried out in the plane-wave Born approximation (PWBA), corrected for the effect of the relativistic motion of the target K-shell electrons,[52] for their polarization and binding energy change by the projectile,[53] and for the Coulomb deflection of the projectile.[52] In such a case the cross section is given by

$$\sigma_K^{\text{ion}} = f^{\text{CD}} f^R \frac{\sigma_{OK}}{\xi\theta_K} F(X,Y) , \tag{A1}$$

where

$$X = \frac{\eta_K}{(\xi\theta_K)^2}, \quad Y = \xi\theta_K ;$$

$$\eta_K = \frac{v_1}{v_2} = 40.32 \frac{E_1 \text{ (MeV)}}{M_1(\text{u}) Z_{2K}^2} .$$

v_1 and v_2 are the projectile and target electron velocities. θ_K is the screening parameter given by the ratio of the true binding energy U_K of the electron in the K shell, and that of the pure hydrogenic system,

$$\theta_K = \frac{U_K \text{ (eV)}}{13.6 Z_{2K}^2} . \tag{A2}$$

Z_{2K} is the target charge corrected for screening:

$$Z_{2K} = Z_2 - 0.3 , \tag{A3}$$

and E_1/M_1 is the projectile energy per nucleon. ξ takes into account the binding energy and polarization effects and is explicitly expressed in Ref. 53. $F(X,Y)$ defines a universal, reduced ionization cross section, tabulated for a

wide range of arguments in Ref. 54.

σ_{OK} is given by

$$\sigma_{OK}=8\pi a_{2K}^2(Z_1/Z_2)^2 , \tag{A4}$$

where $a_{2K}=0.529/Z_{2K}$ (Å) is the target K-shell radius. f^{CD} is a Coulomb deflection factor[51] and f^R is a relativistic correction.[52]

In order to compare the experimental data with the predictions of formula (A1), the experimental K-shell ionization cross sections are reduced to

$$\sigma_K^{red}=\frac{\sigma_K^{exp}}{f^R f^{CD}\sigma_{OK}/(\xi\theta_K)} , \tag{A5}$$

and the calculated σ_K^{red} values are plotted in Fig. 20 vs the reduced energy X. The solid line in this figure is a function $F(X,Y)$ calculated for the constant value $Y=1$. The validity of this comparison is based upon the weak dependence of the function F on the variable Y. This feature of $F(X,Y)$ is discussed in Ref. 55. The K-shell ionization and the K-X production cross section are related by the formula

$$\sigma_K^{ion}=\sigma_{KX}^{prod}\frac{1}{\omega_K} ,$$

where ω_K is the fluorescence yield calculated according to Ref. 56.

The reduced energies of ions employed in this work range from $X=0.05$ to 0.10. It should be noted that numerous experimental results for the K-shell ionization cross section in this region of X were measured on lighter targets and at lower energies than ours.

The difference between the calculated and measured reduced cross sections in Fig. 20 does not exceed 20%, but in the majority of cases the agreement is better than 10%. Therefore it is estimated that the normalization factor employed in the present work is accurate within 20%. This error includes inaccuracy in the presented calculations and also the experimental uncertainties.

---

*Present address: Heavy Ion Laboratory, Warsaw University, Banacha 4, Warsaw, Poland.

†Present address: Institute for Nuclear Sciences, Swierk, Poland.

[1]R. Bass, *Nuclear Reactions with Heavy Ions* (Springer, Berlin, 1980).

[2]J. R. Birkelund and J. R. Huizenga, Annu. Rev. Nucl. Part. Sci. **33**, 265 (1983).

[3]F. S. Stephens, J. R. Leigh, and R. M. Diamond, Nucl. Phys. **A170**, 321 (1971).

[4]H. Ernst, W. Henning, C. N. Davids, W. S. Freeman, T. J. Humanic, F. W. Prosser, and R. A. Racca, Phys. Rev. C **29**, 464 (1984).

[5]D. L. Hillis, J. D. Garret, D. Christensen, B. Fernandez, G. B. Hagemann, B. Herskind, B. B. Back, and F. Folkmann, Nucl. Phys. **A325**, 216 (1979).

[6]J. O. Newton, Phys. Scr. **24**, 83 (1981).

[7]R. Broda, M. Ishihara, B. Herskind, H. Oeschler, S. Ogaza, and H. Ryde, Nucl. Phys. **A248**, 356 (1975).

[8]D. Chmielewska, Z. Sujkowski, J. F. W. Jansen, W. J. Ockels, and M. J. A. de Voigt, Nukleonika **23**, 333 (1978).

[9]J. Dauk, K. P. Lieb, and A. M. Kleinfeld, Nucl. Phys. **A241**, 170 (1975).

[10]A. D'Onofrio, H. Dumont, M. G. Saint Laurent, B. Delaunay, F. Terrasi, and J. Delaunay, Nucl. Phys. **A378**, 111 (1982).

[11]M. A. Xapsos, P. A. De Young, L. J. Satkowiak, and J. J. Kolata, Phys. Rev. C **25**, 2457 (1982).

[12]M. Blann, Nucl. Phys. **80**, 233 (1966).

[13]M. Blann and F. Plasil, University of Rochester Report C00-3494-10, 1973; M. Blann, Report C00-3494-29, 1977; F. Plasil, Oak Ridge National Laboratory Report ORNL/TM-6054, 1977.

[14]A. J. Cole, Institut des Sciences Nucléaires Internal Report 79-14, 1979 (unpublished).

[15]A. J. Cole, N. Longequeue, J. Menet, J. J. Lucas, R. Ost, and B. Viano, Nucl. Phys. **A341**, 284 (1980).

[16]R. Kossakowski, thesis, Grenoble University, 1985.

[17]J. Jastrzębski, R. Kossakowski, J. Łukasiak, M. Moszyński, Z. Preibisz, S. André, A. Gizon, and J. Gizon, Phys. Lett. **97B**, 50 (1980).

[18]J. Jastrzębski, J. Łukasiak, M. Moszyński, Z. Preibisz, J. Gizon, A. Gizon, S. André, and J. Genevey, Proceedings of the International Conference on Large Amplitude Collective Motions, Keszthely, 1979, p. 71.

[19]J. Jastrzębski, R. Kossakowski, J. Łukasiak, M. Moszyński, Z. Preibisz, P. Rymuza, S. André, J. Genevey, A. Gizon, and J. Gizon, Proceedings of the International Conference on Nuclear Behavior at High Angular Momentum, Strasbourg, 1980, p. 139.

[20]R. Kossakowski, J. Jastrzębski, Z. Preibisz, P. Rymuza, W. Skulski, S. André, J. Genevey, A. Gizon, J. Gizon, and V. Barci, Proceedings of the International Conference on Nuclei far from the Stability Line, Helsingør, 1981, CERN Report 81-09, 1981.

[21]A. Pelissier and J. P. Richaud, Institut des Sciences Nucléaires Annual Report, 1980, p. 23.

[22]J. Białkowski, J. Jastrzębski, P. Klepacki, J. Łukasiak, M. Moszyński, Z. Preibisz, W. Skulski, S. André, J. Genevey, A. Gizon, J. Gizon, and G. Margotton, Nucl. Instrum. Methods **204**, 91 (1982).

[23]R. Gunnink and J. B. Niday, University of California Radiation Laboratory Report 51061, 1972, Vol. 1.

[24]Z. Sujkowski and S. Y. van der Werf, Nucl. Instrum. Methods **171**, 445 (1980).

[25]D. Barnéoud, A. Bruder, J. Cl. Dousse, S. Drissi, R. Hayoz, V. Ionescu, J. Kern, and J. A. Pinston, Nuclear Spectroscopy and Muonic Atoms, Progress Report, University of Fribourg, 1983, p. 16.

[26]S. Drissi, S. André, J. Genevey, V. Barci, A. Gizon, J. Gizon, J. A. Pinston, J. Jastrzębski, R. Kossakowski, and Z. Preibisz, Z. Phys. A **302**, 361 (1981).

[27]C. Foin, S. André, and D. Barnéoud, Nucl. Phys. **A289**, 77 (1977).

[28]C. Foin, S. André, J. Genevey, S. Drissi, V. Ionescu, J. Kern, and M. Rast, Nucl. Phys. **A417**, 511 (1984).

[29]*Table of Isotopes*, 7th ed., edited by C. D. Lederer and V. S. Shirley (Wiley, New York, 1978).

[30]U. Reus and W. Westmeier, At. Data Nucl. Data Tables **29**, 1 (1983).

[31]F. Beck, J. Błocki, M. Dworzecka, and G. Wolschin, Phys.

Lett. **76B**, 35 (1978).
[32]J. R. Birkelund, L. E. Tubbs, J. R. Huizenga, J. N. De, and D. Sperber, Phys. Rep. **56**, 107 (1979).
[33]H. J. Krappe, J. R. Nix, and A. J. Sierk, Phys. Rev. C **20**, 992 (1979).
[34]J. Błocki, private communication.
[35]D. G. Sarantites, L. Westerberg, M. L. Halbert, R. A. Dayras, D. C. Hensley, and J. H. Barker, Phys. Rev. C **18**, 774 (1978).
[36]J. C. Beene, M. L. Halbert, D. C. Hensley, R. A. Dayras, K. Geoffroy Young, D. G. Sarantites, and J. H. Barker, Phys. Rev. C **23**, 2463 (1981).
[37]J. R. Leigh, D. J. Hinde, J. O. Newton, W. Galster, and S. H. Sie, Phys. Rev. Lett. **48**, 527 (1982).
[38]H. C. Britt, B. H. Erkkila, P. D. Goldstone, R. H. Stokes, B. B. Back, F. Folkmann, O. Christensen, B. Fernandez, J. D. Garrett, G. B. Hagemann, B. Herskind, D. L. Hillis, F. Plasil, R. L. Ferguson, M. Blann, and H. H. Gutbrod, Phys. Rev. Lett. **39**, 1458 (1977).
[39]H. Morgenstern, W. Bohne, K. Grabisch, H. Lehr, and W. Stoffler, Z. Phys. A **313**, 39 (1983).
[40]A. C. Xenoulis, A. E. Aravantinos, C. J. Lister, J. W. Olness, and R. L. Kozub, Phys. Lett. **106B**, 461 (1981).
[41]F. Plasil, R. L. Ferguson, R. L. Hahn, E. Obenshain, F. Pleasonton, and G. R. Young, Phys. Rev. Lett. **45**, 333 (1980).
[42]D. W. Lang, Nucl. Phys. **77**, 545 (1966).
[43]A. Gilbert and A. G. W. Cameron, Can. J. Phys. **43**, 1446 (1965).
[44]J. R. Grover and J. Gilat, Phys. Rev. **157**, 802 (1967); **157**, 815 (1967); **157**, 823 (1967).
[45]C. M. Perey and F. G. Perey, Nucl. Data Tables **17**, 1 (1976).
[46]J. Wilczyński, K. Siwek-Wilczyńska, J. Van Driel, S. Gonggrijp, D. C. J. Hageman, R. V. F. Janssens, J. Łukasiak, R. J. Siemssen, and S. Y. van der Werf, Nucl. Phys. **A373**, 109 (1982).
[47]S. André, V. Barci, D. Barnéoud, R. Béraud, A. Charvet, H. El-Samman, J. Genevey, A. Gizon, J. Gizon, R. Kossakowski, J. Treherne, and B. Weiss, Z. Phys. A **308**, 181 (1982).
[48]J. Kropp, M. Klewe-Nebenius, H. Faust, J. Buschmann, H. Rebel, H. J. Gils, and K. Wisshak, Z. Phys. A **280**, 61 (1977).
[49]R. K. Gardner and T. J. Gray, At. Data Nucl. Data Tables **21**, 515 (1978).
[50]G. Bissinger, P. H. Nettles, S. M. Shafroth, and A. W. Waltner, Phys. Rev. A **10**, 1932 (1974).
[51]R. Anholt, Phys. Rev. A **17**, 983 (1978).
[52]P. A. Amundsen, L. Kocbach, and J. M. Hansteen, J. Phys. (London) **B9**, L203 (1976).
[53]G. Basbas, W. Brett, and R. Laubert, Phys. Rev. A **17**, 1655 (1978).
[54]R. Rice, G. Basbas, and F. D. McDaniel, At. Data Nucl. Data Tables **20**, 503 (1977).
[55]C. E. Merzbacher and H. W. Lewis, in *Handbuch der Physik,* edited by S. Flügge (Springer, Berlin, 1958), Vol. 34, p. 166.
[56]W. Bambynek, B. Crasemann, R. W. Fink, H. U. Freund, H. Mark, C. D. Swift, R. E. Price, and P. V. Rao, Rev. Mod. Phys. **44**, 716 (1972).